Supporting Information

Simultaneously Suppressing Lithium Dendrites Growth and Mn Dissolution by Integration of a Safe Inorganic Separator in $LiMn_2O_4$/Li Battery

Zhixiang Rao,‡[a,b] Ze Yang,‡[b,c] Wenzhe Gong,[b] Shang Su,[b] Qiuyun Fu*[a] and Yunhui Huang*[b]

[a] School of Optical and Electronic Information, Engineering Research Center for Functional Ceramics of the Ministry of Education, Huazhong University of Science and Technology, Wuhan, Hubei, 430074, China

[b] State Key Laboratory of Material Processing and Die & Mould Technology, School of Materials Science and Engineering, Huazhong University of Science and Technology, Wuhan, Hubei, 430074, China

[c] Institute of Nanoscience and Nanotechnology, College of Physical Science and Technology, Central China Normal University, Wuhan, Hubei, 430079, China

‡The authors contributed equally.

Corresponding Author

*E-mail: huangyh@hust.edu.cn (Y. H. Huang).

*E-mail: fuqy@hust.edu.cn (Q. Y. Fu).

Table S1 Physical properties of the HAP and PP separators

Separator	Thickness (μm)	Porosity (%)	Electrolyte uptake (%)	Ionic conductivity (mS cm^{-1})
PP	25	43	129	0.82
HAP	65	84	262	2.6

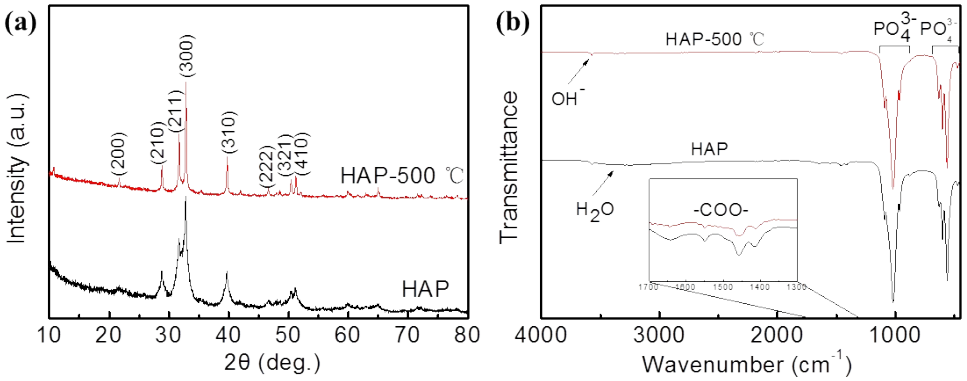

Figure S1 (a) XRD patterns and (b) FTIR spectra of the as-prepared HAP nanowires and the sample after treatment at 500 °C.

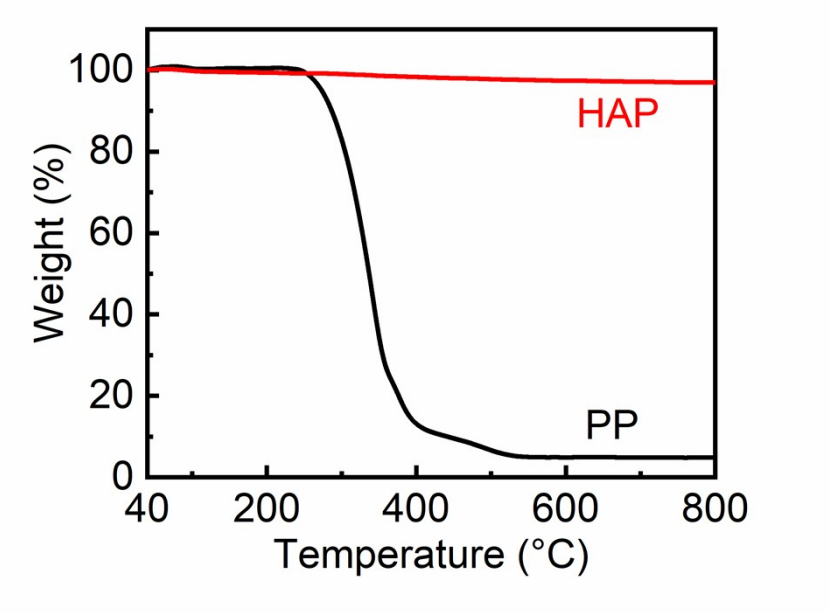

Figure S2 TG curves of the HAP and PP separators.

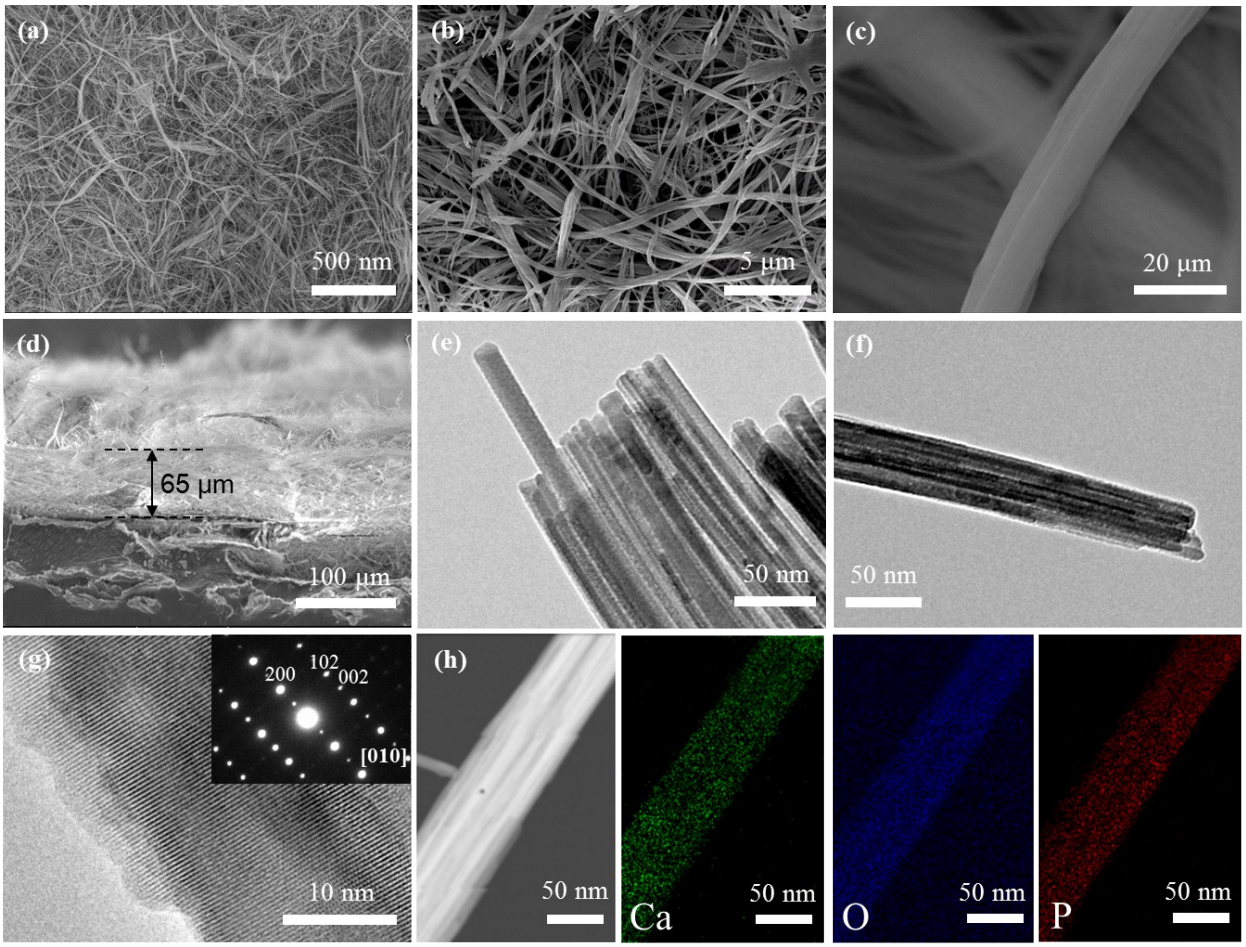

Figure S3. (a-c) SEM images of the surface of the HAP separator at different magnifications. (d) Cross-section of the HAP separator. (e-g) High-resolution TEM image and corresponding SAED pattern of the HAP nanowires. (h) STEM dark-field images of the as-prepared HAP nanowires and the corresponding EDX element mapping of Ca, O and P.

Figure S1 and S3 demonstrate the phase information and microstructure morphology of the as-prepared HAP nanowires. Figure S1a shows the XRD patterns of the HAP separator. The peaks at 21.8°, 28.9°, 31.8°, 32.9°, 39.8° 46.7°, 50.5°, 51.3° correspond to (200), (210), (211), (300), (310), (222), (321), (410) crystal planes of hydroxyapatite ($Ca_{10}(PO_4)_6(OH)_2$, PDF#54-0022), respectively, which prove the crystal structure of the HAP nanowires. The phase structure of the HAP nanowires is further confirmed by FT-IR, as shown in Figure S1b. The absorption peaks at

1089, 1018, 962, 629, 599 and 558 cm^{-1} are attributed to PO_4^{3-} ions in HAP, and the sharp peak at 3571 cm^{-1} can be ascribed to stretching mode of the -OH group in HAP.[1] The broad band besides the hydroxyl group and the small peaks at 1600-1400 cm^{-1} are derived from absorbed water and $–COO^–$ in oleic acid, respectively.[1, 2] According to the SEM images (Figure S3a, b), the length of the HAP nanowires are dozens of micrometers. The nanowires cross-link with each other to form a porous, flexible network. The high magnification image (Figure S3c) indicates that the diameters of HAP nanowires are about 200-300 nm. The uniform, porous separator can be prepared by a simple vacuum suction filtration method, and the thickness can be controlled by adjusting the amount of HAP nanowires. Generally speaking, a thinner separator can enhance the energy density of the batteries. The thickness of the HAP separator employed in this work is about 65 μm, as shown in Figure S3d. The TEM images (Figure S3e-g) further indicate that the nanowires are composed of several thinner monocrystalline nanowires with diameter of 10-20 nm. Such self-assembled nanowires have been proven more flexible compared to the single nanowires[3] which is beneficial for the high flexibility of the HAP separator. High-resolution TEM (HRTEM) image displays clear and continues lattice planes (Figure S3g), indicative of high crystallinity of the HAP nanowires. The selected area electron diffraction (SAED) pattern shown in the inset of Figure 1g reveals the highly ordered single-crystalline nature of HAP nanowires, which can be indexed to the [010] zone axis. Figure S3h show the STEM dark field image of a HAP nanowire and the corresponding energy dispersive X-ray (EDX) elemental mapping results indicate the uniform distribution of Ca, O, and P elements.

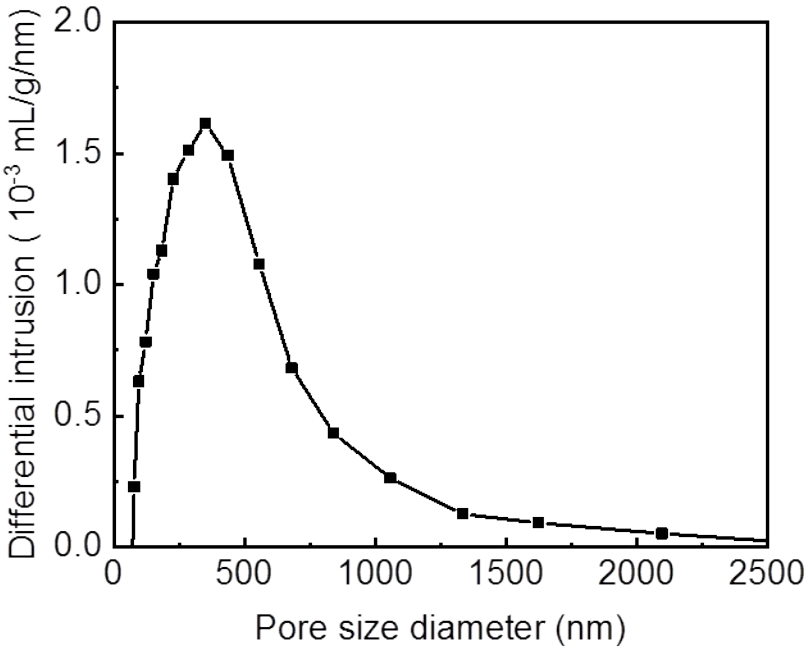

Figure S4 Pore size distribution curves of the HAP separator

Figure S4 shows the pore size distribution curves of the HAP separator obtained by Mercury Intrusion Porosimetry. The average pore size of the separator is about 350 nm. The pores from the HAP separator are irregularly formed among the ceramic nanowires. The porosity of the HAP separator is 80% which is much larger than the PP separator than the PP separator (43%). It means the HAP separator can absorb more electrolyte.

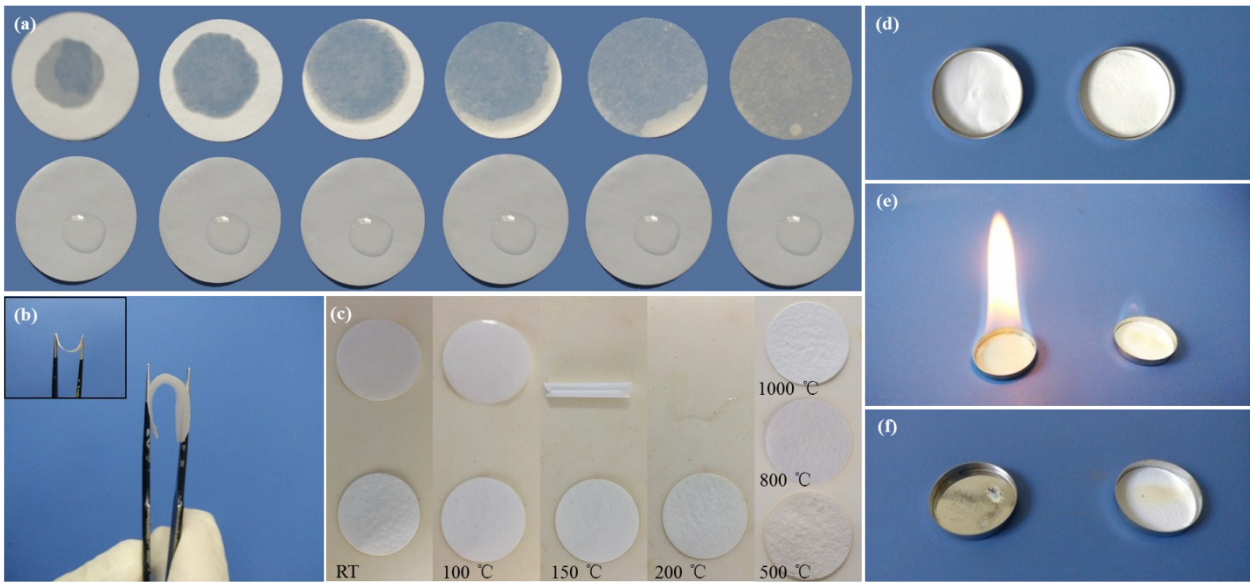

Figure S5 (a) Optical images of the HAP (upper part) and PP separator (bottom part) after dripping a drop of electrolyte for 0, 5, 10, 20, 30, 60 seconds. (b) Flexibility demonstration of the HAP separator (inset: HAP separator after 1000 ℃ treatment). (c) Illustration of thermal shrinkage of the separators at various temperature (upper part: PP separator, bottom and right part: HAP separator).

Commercial PP separators usually suffer from poor electrolyte wettability due to their incompatibility with polar liquid electrolytes and low surface energies that restrict the rate capability in lithium based batteries. Moreover, the battery manufacturing process is also a key point.[4] To study the wettability difference between the HAP separator and PP separator, a drop of electrolyte was dripped onto the separators. Figure S5a shows the optical images of the separators after dripping for 0, 5, 10, 20, 30, 60 seconds, respectively. It is clearly observed that the electrolyte on PP separator only spread out or infiltrate into the membrane, demonstrating a poor compatibility with electrolyte. On the contrary, the HAP separator absorbs the electrolyte and gets fully infiltrated within one minute. The superior electrolyte affinity of the HAP separator compared to the PP separator results from the synergistic effect between favorable

compatibility to the electrolyte and the highly porous structure. Figure S5b demonstrates the flexibility of the HAP separator. The membrane overcomes the fragile character of ceramic materials, and can be rolled up and bent to over 180°, which is even comparable to polyolefin materials.

The thermal stability also plays an important role in LIBs and LMBs, especially for the high-power and high-energy batteries.[5-8] High-temperature induced thermal shrinkage of separators cannot segregate the cathode and anode any more, which may lead to short circuit and even fire or explosion. As observed in Figure S5c, the PP separator begins to soften at 100 °C, then severely rolls up and shrinks at 150 °C. When the temperature rises to 200 °C, it completely decomposes and leaves almost nothing. In comparison, the HAP separator maintains its structure and exhibits nearly no shrinkage at 500, 800 and even 1000 °C. Besides, thermogravimetric (TG) measurement was also carried out to testify thermal properties of the separators. In Figure S2, PP sample starts to decompose when the temperature increases to 250 ℃，and is completely burnt out at 530 ℃, while the HAP sample shows ultrahigh stability even at 800 ℃ with nearly no mass loss. Moreover, the HAP separator still keeps a high flexibility after 1000 °C heat treatment (inset in Figure S5b), which benefits from the high thermal and chemical stability of hydroxyapatite as well as the superior structure of the HAP nanowires. The chemical stability is further confirmed by XRD and FTIR results. The diffraction peaks obtained at 500 °C show exactly the same position but sharper shape as compared to those at room temperature. This implies that the HAP nanowires are very stable at high temperature, which is further proven by the corresponding FTIR curves (Figure S1b). As is well known, except for short circuit, the high flammability of the electrolytes, especially the ether-based electrolytes, is another obstacle for the safety of LIBs and LMBs.[9-11] In consideration of the organic characters of the polyolefin

separators, the battery would fail rapidly once the thermal runaway happens, which induces fire or explosion.

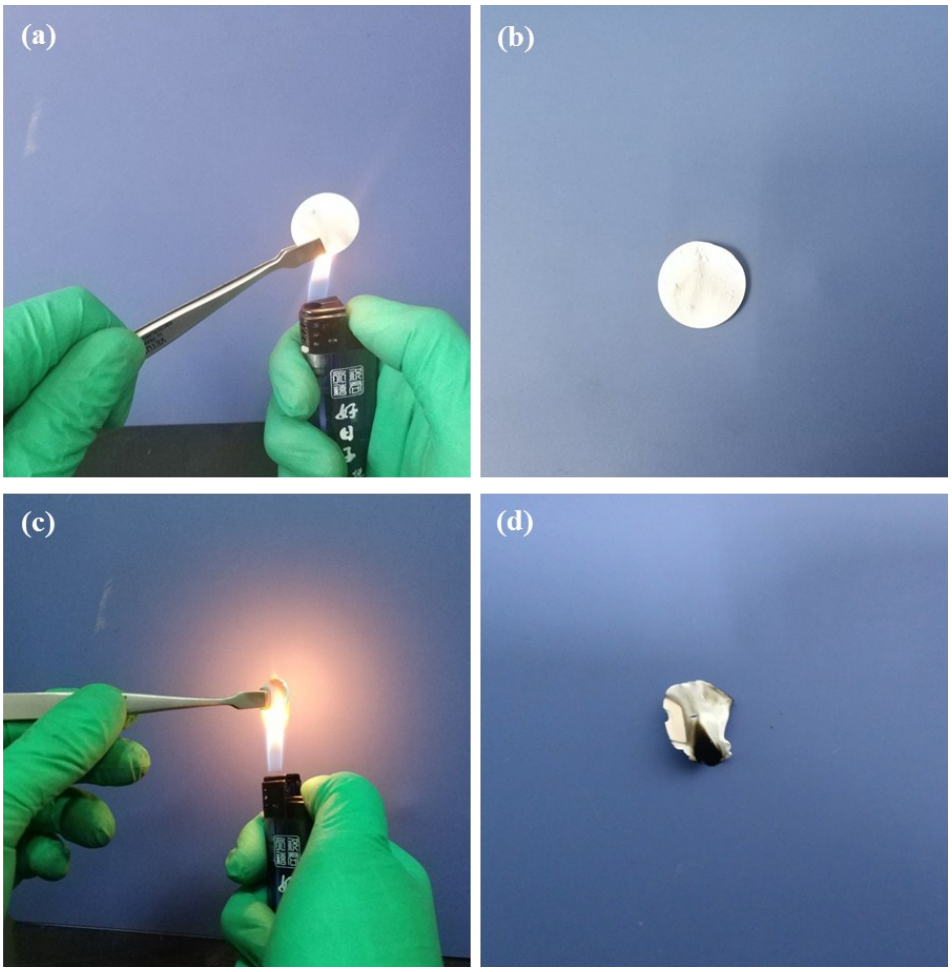

Figure S6 Optical images of the HAP separator (a) before and (b) after burning and Optical images of the HAP/cellulose separator (c) before and (d) after burning

To test the fire-resistant performance of the separators, a drop of 1, 3-dioxolane was dripped on them, after fully wetting, the separators were ignited with a lighter. This process is recorded in Figure S5. The PP separator burns quickly with a huge flame and nothing exists in the cell, whereas the HAP separator shows a much smaller flame and does not have any shrinkage after burning. The excellent fire-resistant performance benefits from the ultrahigh thermal stability and the superb wettability to electrolyte of the HAP nanowires.

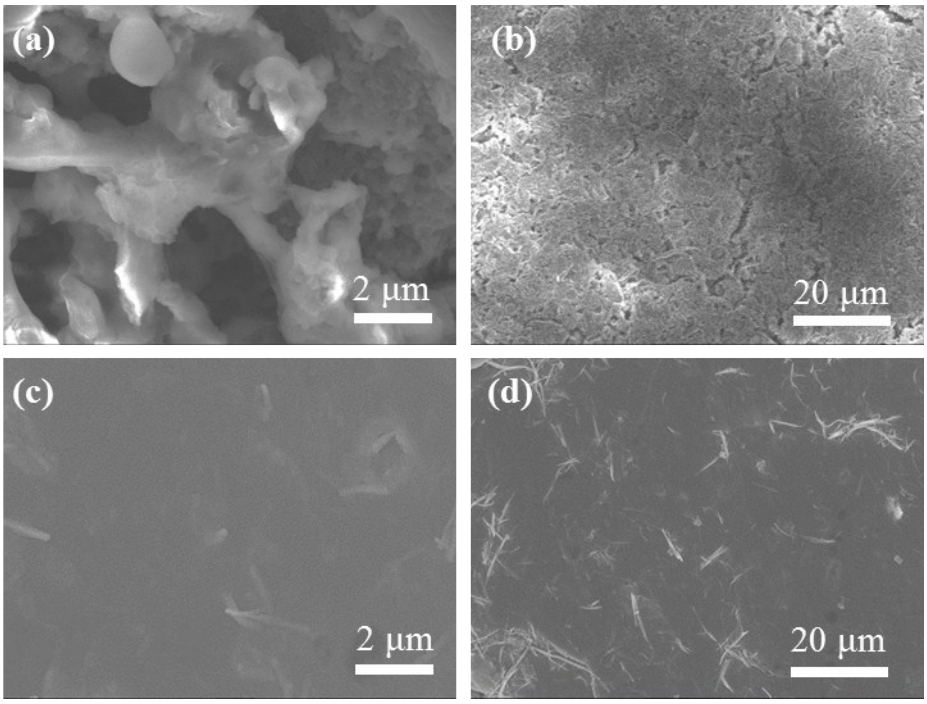

Figure S7. SEM images of the Lithium metal electrode after 20 plating/stripping cycles with (a, b) PP separator and (c, d) HAP separator, respectively. The current density was fixed at 1 mA cm^{-2} whereas the capacity was set at 1 mA h cm^{-2}.

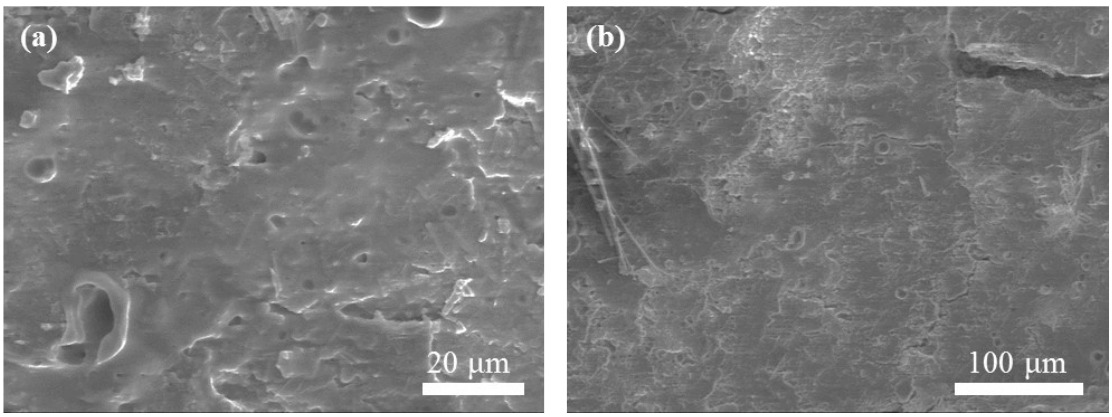

Figure S8. SEM images of the Lithium metal electrode after 100 plating/stripping cycles HAP separator. The current density was fixed at 1 mA cm^{-2} whereas the capacity was set at 1 mA h cm^{-2}.

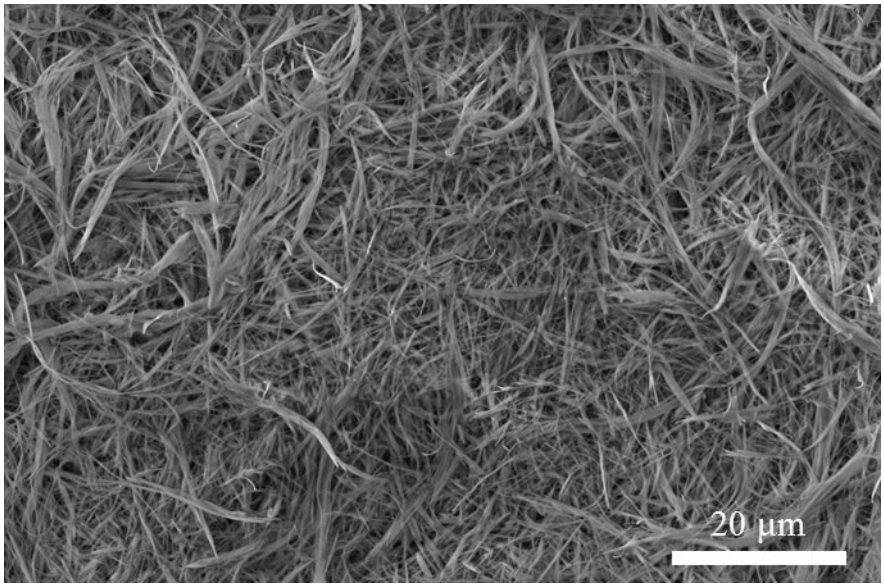

Figure S9. SEM images of the HAP separator after 20 plating/stripping cycles. The current density was fixed at 1 mA cm^{-2} whereas the capacity was set at 1 mA h cm^{-2}.

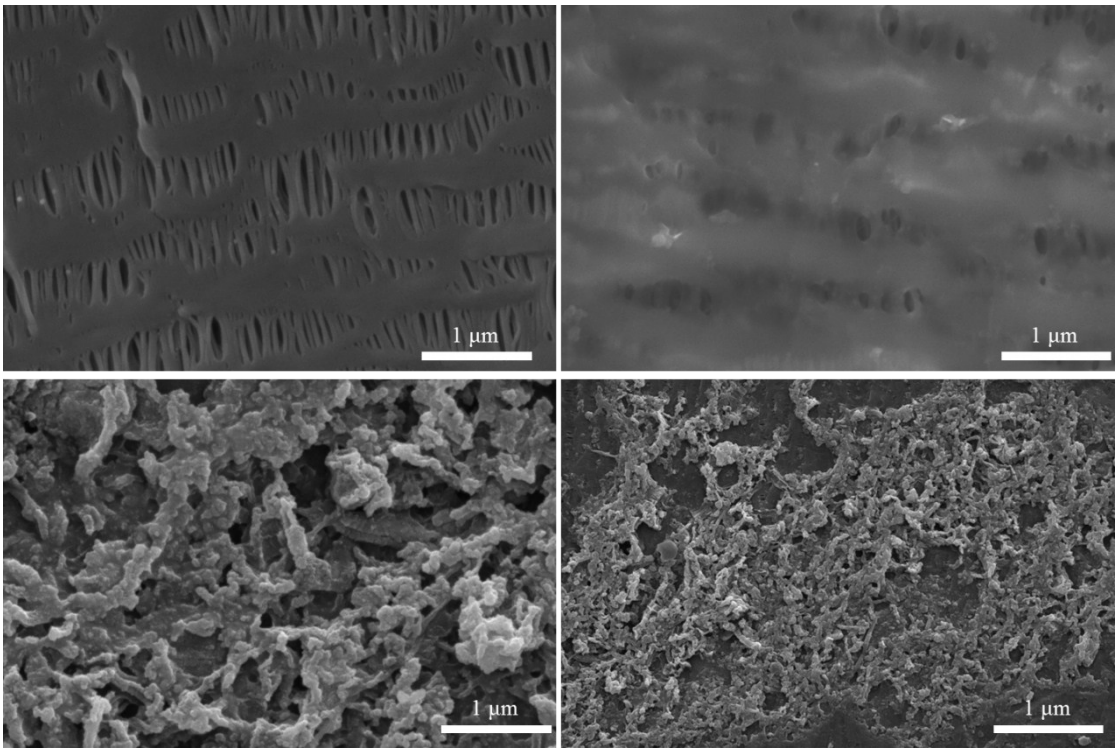

Figure S10. SEM images of the PP separator (a) before and (b-d) after 20 plating/stripping cycles. The current density was fixed at 1 mA cm^{-2} whereas the capacity was set at 1 mA h cm^{-2}.

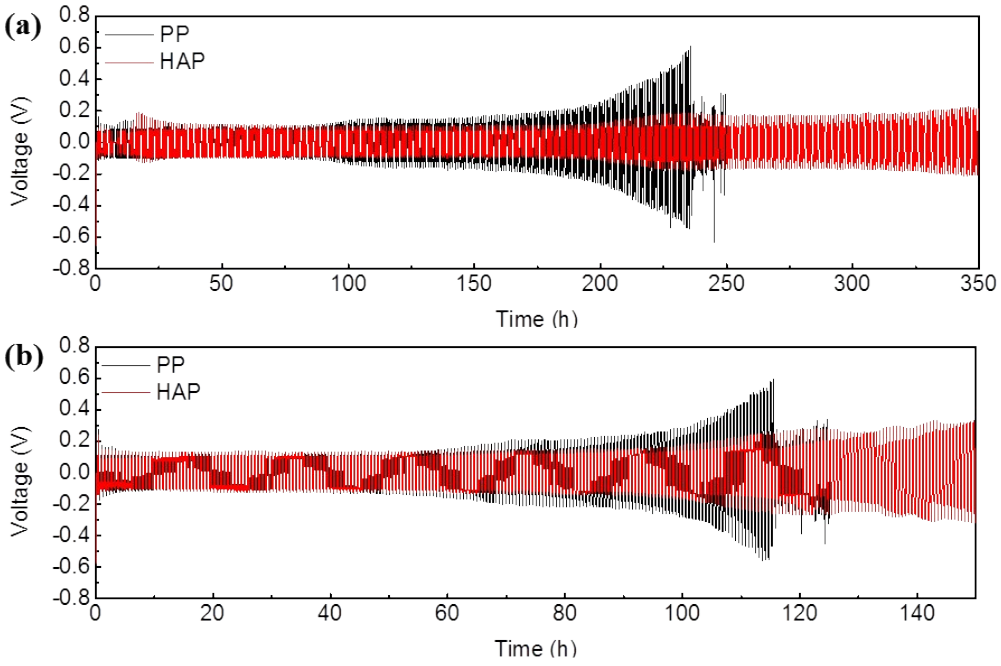

Figure S11. Voltage–time profiles of the Li plating/stripping process with a cycling capacity of 1 mA h cm^{-2} at (a) 2 mA cm^{-2}, (b) 4 mA cm^{-2} in symmetric Li|separator|Li cells.

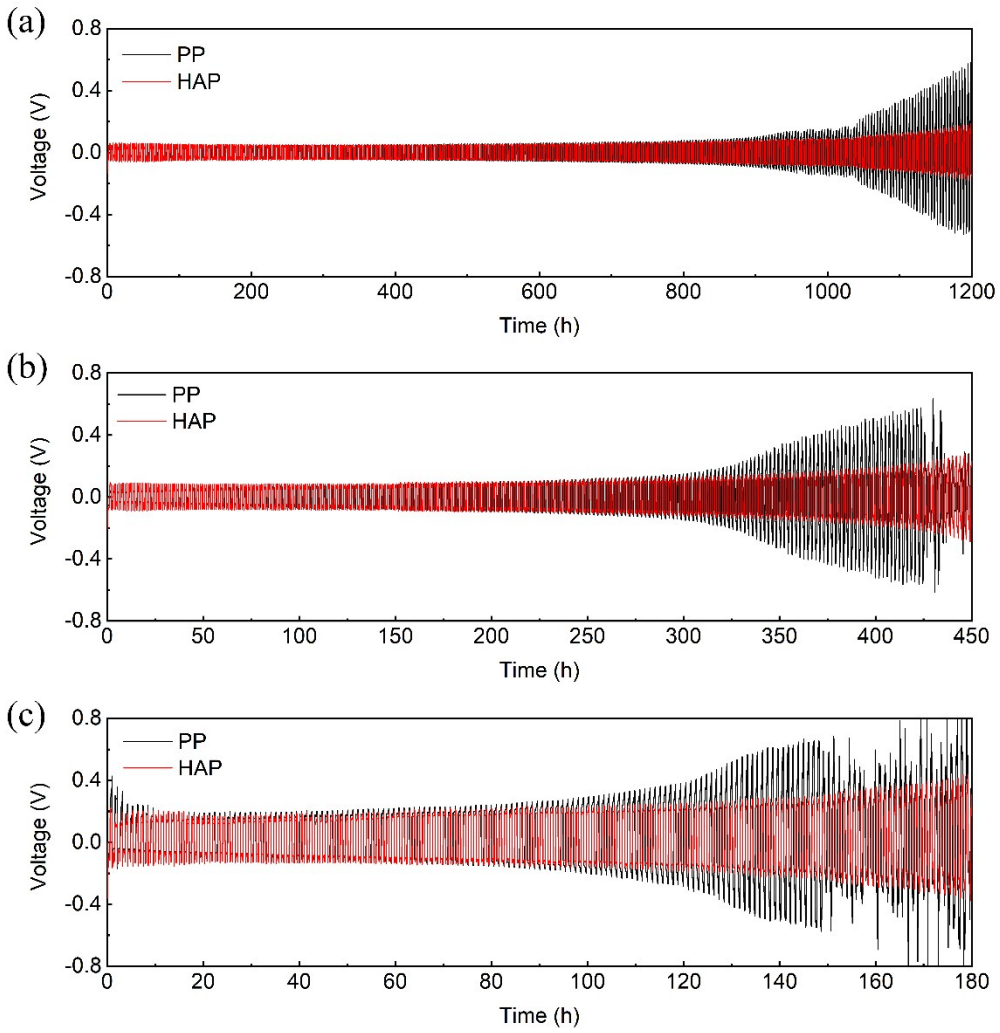

Figure S12. Voltage–time profiles of the Li plating/stripping process with a cycling capacity of 1 mA h cm^{-2} at (a) 0.5 mA cm^{-2}, (b) 1 mA cm^{-2} and (c) 2mA cm^{-2} in symmetric Li|separator|Li cells, the electrolyte was 1 M $LiPF_6$ in 1:1 v/v EC/DEC.

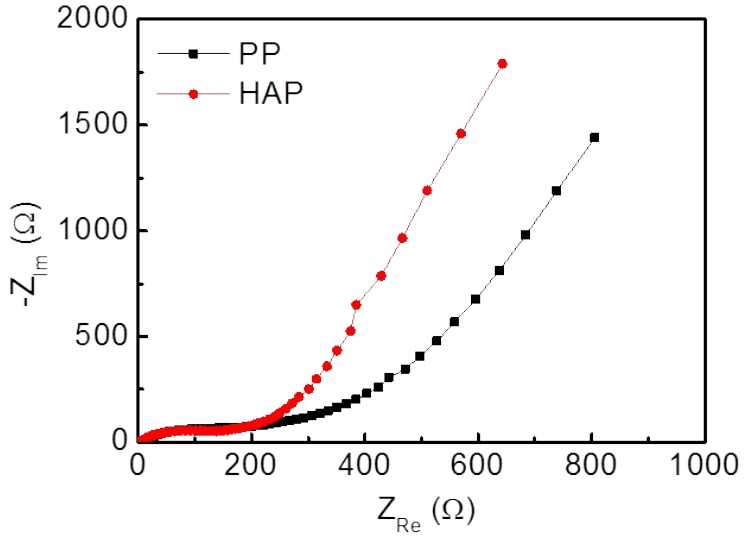

Figure S13. Electrochemical impedance spectra of symmetric Li|separator|Li cells with PP and HAP separators.

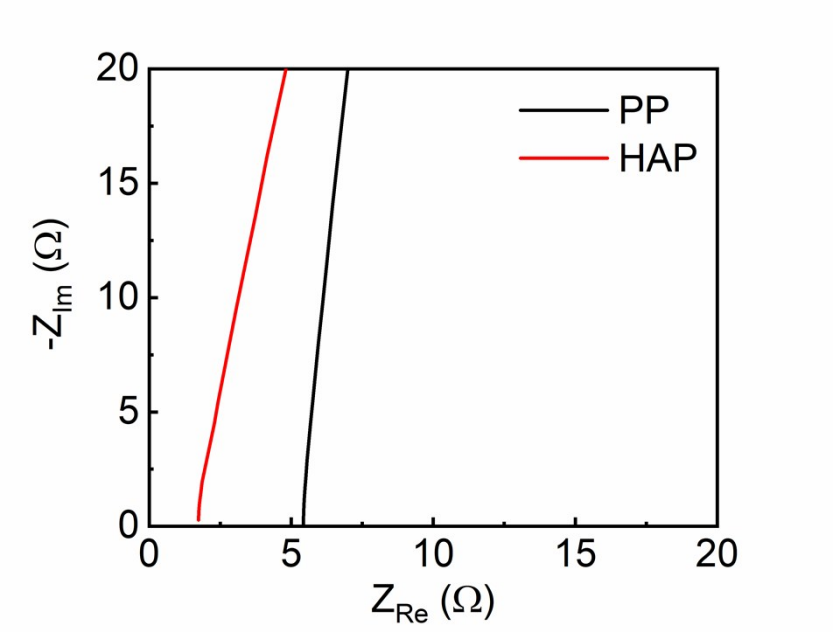

Figure S14 Nyquist plots of the HAP and PP separators.

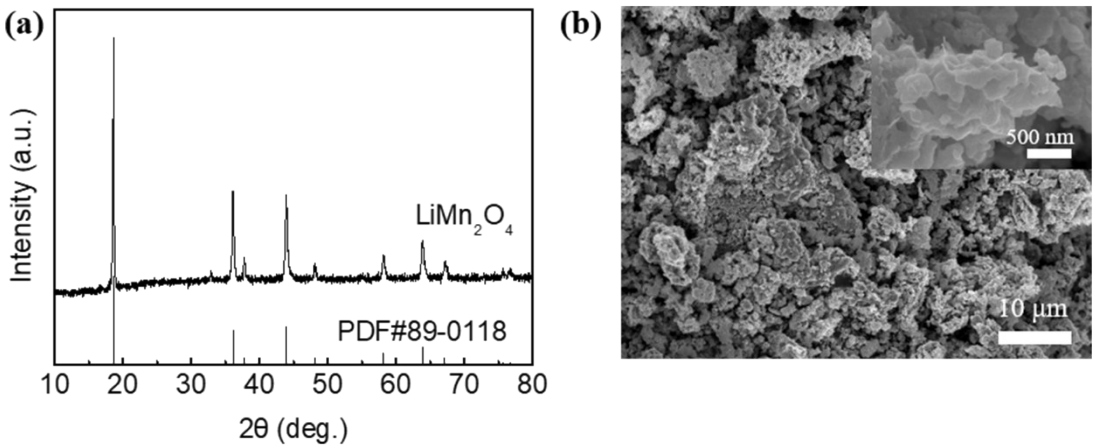

Figure S15. (a) XRD pattern and (b) SEM image of the sample $LiMn_2O_4$.

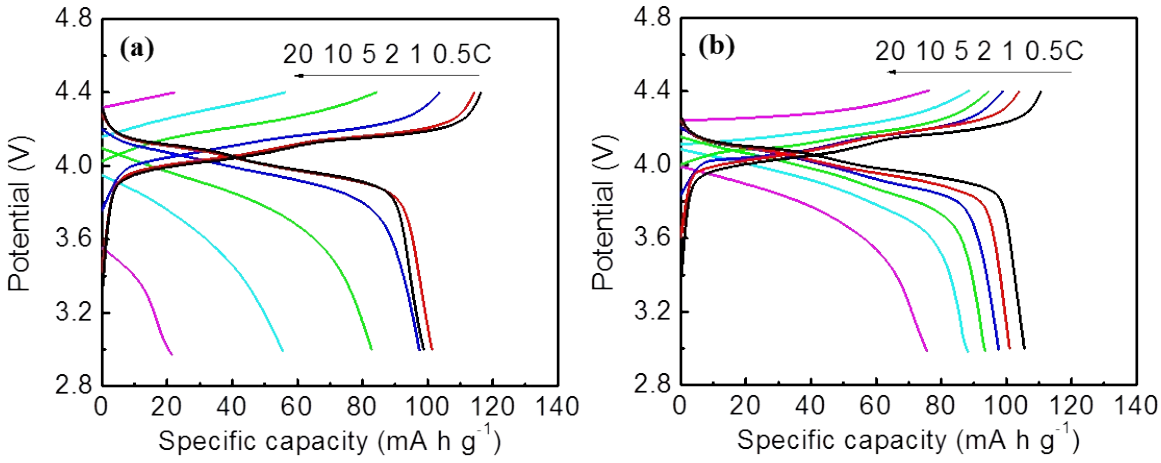

Figure S16. Charging and discharging profiles of $LiMn_2O_4$ cathode with (a) PP and (b) HAP separators.

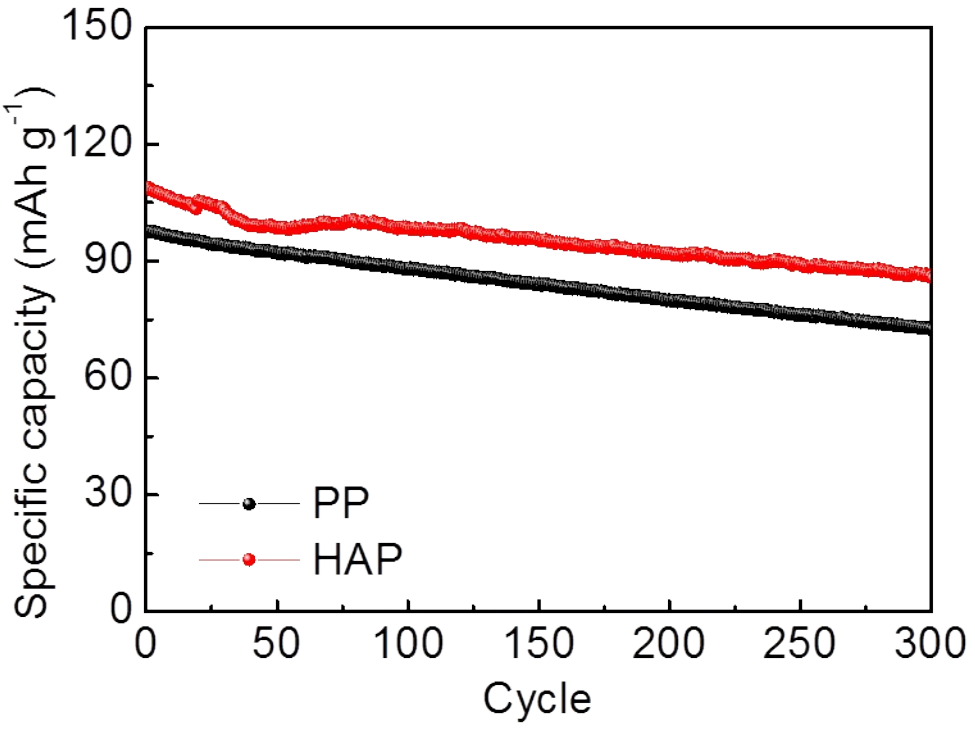

Figure S17. Cyclic performances of $LiMn_2O_4$ cathode with (a) PP and (b) HAP separators.

References

1. T. W. Sun, Y. J. Zhu and F. Chen, *Chem. Eur. J.*, 2017, **23**, 3850-3862.
2. X. Wang, J. Zhuang, Q. Peng and Y. D. Li, *Advanced Materials*, 2006, **18**, 2031-2034.
3. H. Li, Y.-J. Zhu, Y.-Y. Jiang, Y.-D. Yu, F. Chen, L.-Y. Dong and J. Wu, *ChemNanoMat*, 2017, **3**, 259-268.
4. J. Dai, C. Shi, C. Li, X. Shen, L. Peng, D. Wu, D. Sun, P. Zhang and J. Zhao, *Energy & Environmental Science*, 2016, **9**, 3252-3261.
5. L. Ma, R. Chen, Y. Hu, W. Zhang, G. Zhu, P. Zhao, T. Chen, C. Wang, W. Yan, Y. Wang, L. Wang, Z. Tie, J. Liu and Z. Jin, *Energy Storage Materials*, 2018, **14**, 258-266.
6. G. Feng, Z. Li, L. Mi, J. Zheng, X. Feng and W. Chen, *Journal of Power Sources*, 2018, **376**, 177-183.
7. J. K. Kim, D. H. Kim, S. H. Joo, B. Choi, A. Cha, K. M. Kim, T. H. Kwon, S. K. Kwak, S. J. Kang and J. Jin, *ACS nano*, 2017, **11**, 6114-6121.
8. D. Lin, D. Zhuo, Y. Liu and Y. Cui, *Journal of the American Chemical Society*, 2016, **138**, 11044-11050.
9. K. Liu, W. Liu, Y. Qiu, B. Kong, Y. Sun, Z. Chen, D. Zhuo, D. Lin and Y. Cui, *Science advances*, 2017, **3**, e1601978.
10. P.-H. Huang, S.-J. Chang and C.-C. Li, *Journal of Power Sources*, 2017, **338**, 82-90.
11. Q. Wang, P. Ping, X. Zhao, G. Chu, J. Sun and C. Chen, *Journal of Power Sources*, 2012, **208**, 210-224.